

Retrieval-Augmented Perception: High-Resolution Image Perception Meets Visual RAG

Wenbin Wang¹ Yongcheng Jing² Liang Ding³ Yingjie Wang²
Li Shen⁴ Yong Luo¹ Bo Du¹ Dacheng Tao²

Abstract

High-resolution (HR) image perception remains a key challenge in multimodal large language models (MLLMs). To overcome the limitations of existing methods, this paper shifts away from prior dedicated heuristic approaches and revisits the most fundamental idea to HR perception by enhancing the long-context capability of MLLMs, driven by recent advances in long-context techniques like retrieval-augmented generation (RAG) for general LLMs. Towards this end, this paper presents the first study exploring the use of RAG to address HR perception challenges. Specifically, we propose **Retrieval-Augmented Perception (RAP)**, a training-free framework that retrieves and fuses relevant image crops while preserving spatial context using the proposed *Spatial-Awareness Layout*. To accommodate different tasks, the proposed *Retrieved-Exploration Search (RE-Search)* dynamically selects the optimal number of crops based on model confidence and retrieval scores. Experimental results on HR benchmarks demonstrate the significant effectiveness of **RAP**, with LLaVA-v1.5-13B achieving a 43% improvement on *V* Bench* and 19% on *HR-Bench*. Code will be available at <https://github.com/DreamMr/RAP>.

1. Introduction

Multimodal large language models (MLLMs) have achieved remarkable progress in vision-language understanding, reasoning, and interaction, leveraging visual signals to process and interpret visual information (Yin et al., 2023). Current MLLMs (Liu et al., 2024a; Bai et al., 2023; Liu et al., 2024b; Wang et al., 2023a; Abdin et al., 2024) typically process im-

¹Wuhan University ²Nanyang Technological University ³The University of Sydney ⁴Shenzhen Campus of Sun Yat-sen University.

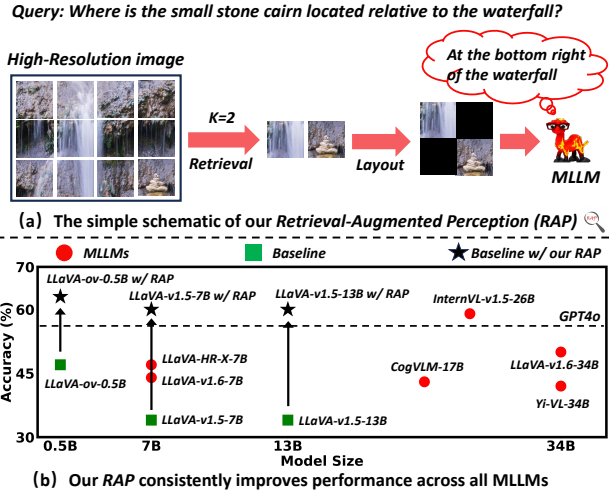


Figure 1. (a) Overview of the proposed **Retrieval-Augmented Perception (RAP)** framework, which divides the HR images into image crops for retrieval, followed by layout reconstruction to retain the spatial information; (b) Performance comparison of MLLMs across various model sizes, demonstrating consistent improvements with our **RAP** on *HR-Bench*.

ages at a fixed resolution (e.g., 448×448). While this design streamlines the computational pipeline, it introduces significant challenges, such as shape distortion and blurring when handling high-resolution (HR) images. These distortions notably impair the performance of MLLMs, especially in tasks that involve analysing real-world images with varying resolutions, such as visual grounding and optical character recognition that demand fine-grained visual details (Zhang et al., 2024a; Jing et al., 2023; Wang et al., 2024b; Jing et al., 2021b; Zhang et al.; Wang et al., 2024d; 2025).

In response to this dilemma, emerging research on enhancing the HR image perceptual capabilities of MLLMs has gained increasing attention. Existing approaches can be broadly categorised into three groups: (1) cropping-based methods (Chen et al., 2024b; Liu et al., 2024b; Li et al., 2024c), (2) HR visual encoder methods (Luo et al., 2024; Ge et al., 2024; Lu et al., 2024), and (3) search-based meth-

ods (Wu & Xie, 2024; Wang et al., 2024c; Shen et al., 2024). Despite notable progress, both cropping-based and HR visual encoder methods still require downsampling HR images to mitigate excessively long visual token sequences, resulting in substantial loss of fine-grained details. Although search-based methods avoid downsampling, they face several limitations. These methods follow a top-down search from high to low resolution; however, at the initial stage, models struggle to accurately perceive small objects (Wang et al., 2024c), often resulting in erroneous search paths.

These limitations prompt our rethinking of the fundamental challenge in HR perception. Ideally, effective HR perception requires an MLLM with robust long-context capabilities—for instance, processing an 8K HR image with ViT-L/14 (Dosovitskiy et al., 2021) generates approximately $\sim 300K$ visual tokens. This raises the question of whether the key to HR perception lies in enhancing the long-context capacity of MLLMs, rather than solely relying on existing heuristic approaches, particularly in light of recent encouraging advancements in long-context techniques for general LLMs. In particular, retrieval-augmented generation (RAG) has proven highly effective in recent long-context LLMs, by retrieving crucial fragments and reducing the impact of irrelevant information (Jin et al., 2024). Motivated by this, this paper poses a largely overlooked question: *Is it possible to directly enhance the long-context capability of MLLMs using RAG, as in general LLMs, to overcome the limitations of existing HR perception methods?*

However, exploring this research question presents significant challenges, as images, unlike text, are two-dimensional (excluding the channel dimension) and are characterised by width and height. As a pilot study, we begin by focusing on two key aspects: the layout of retrieved image crops and the impact of the number of retrieved crops on performance. This leads to the following specific challenges: **1) How should the retrieved image crops be organised?** Furthermore, the number of retrieved key fragments plays a critical role in RAG performance (Jin et al., 2024), prompting our second research question: **2) How does the number of retrieved image crops influence the final performance?** Building on insights from these two questions, we further pose a third research question: **3) How can RAG systems be designed to enhance MLLM perception of HR images?**

To address the **1st challenge**, we conduct a series of experiments using the **HR-Bench** (Wang et al., 2024c) and **V* Bench** (Wu & Xie, 2024) to investigate the effects of different layout strategies. We evaluate state-of-the-art (SOTA) MLLMs (Liu et al., 2024a;b) across various layout configurations. Specifically, we compare three strategies: 1) ordering them in ascending order based on retrieval scores (Jin et al., 2024), 2) arranging the retrieved image crops in their original order, and 3) preserving the relative positional rela-

tionships among the retrieved crops. Our empirical results suggest that maintaining the relative positional relationships of the image crops significantly enhances HR perception, particularly for tasks that depend on spatial relationships.

In response to the **2nd question**, this paper investigates the impact of the number of retrieved image crops. Our findings reveal that the optimal number of retrieved crops depends on the task type. For single-instance perception tasks, a small number of crops suffices for significant performance improvements, whereas too many crops degrade performance due to the high image resolution. In contrast, for cross-instance perception tasks, fewer crops result in information loss and reduced performance, while more crops help preserve essential details and minimise performance degradation. However, an excessive number of crops still harms performance due to challenges from overly high resolution.

In tackling the **3rd question**, we integrate the insights gained from the previous investigations to design a new framework, which we term **Retrieval-Augmented Perception (RAP)**. As illustrated in Figure 1(a), **RAP** processes high-resolution images by retrieving image crops relevant to the query through VisRAG (Yu et al., 2024). We propose a simple yet efficient layout method, termed as *Spatial-Awareness Layout*, which preserves the original relative spatial relationships among the image crops. To determine the optimal number of retrieved image crops, we introduce a novel scheme termed as *RE-Search (Retrieved-Exploration Search)*, which adaptively adjusts the number of crops based on the model’s confidence in the sufficiency of the retrieved information.

In particular, VisRAG is first used to compute the similarity scores between each image crop and the query. We then retain the top K crops with the highest similarity scores, ensuring their relative spatial relationships are preserved through the *Spatial-Awareness Layout*. To determine the optimal K , we construct a RE-Tree, where each node represents a new image synthesized by retaining different proportions of the image crops. The search process within this tree is guided by both the retrieved similarity scores and the model’s confidence in whether the image offers sufficient information to answer the query.

In sum, our main contributions are as follows:

- To the best of our knowledge, this is the first study exploring using visual RAG to enhance HR image perception in MLLMs. Our findings highlight the critical role of preserving the spatial information of retrieved image crops and the varying number of crops required depending on task types.
- We propose **RAP**, a training-free framework that comprises *Spatial-Awareness Layout* to preserve the positions of image crops and *RE-Search* to adaptively select the optimal number of retained crops.

- Experiments demonstrate that *RAP* consistently delivers significant improvements, with an average accuracy increase of 24% on HR image benchmarks and even general MLLM benchmarks.

2. Related Work

MLLMs consist of a **Visual Encoder** (Dosovitskiy et al., 2021; Radford et al., 2021; Jing et al., 2021a) for extracting visual features and a **LLM** (Touvron et al., 2023a;b) for decoding text, both initialized from pretrained models. A **multimodal Connector** (e.g., MLP) links the vision and language modalities (Wang et al., 2024a; Rao et al., 2022; Wang et al., 2023b). To align the resolution used during visual encoder pretraining (e.g., 336×336 in LLaVA), images are typically resized, which can distort and blur HR images. To address this, existing approaches fall into three categories: **1) cropping-based methods**, **2) HR visual encoder methods**, and **3) search-based methods**.

Cropping-Based Methods. Representative cropping-based methods for HR MLLMs (Chen et al., 2024a; Zhang et al., 2024b; Liu et al., 2024c), such as LLaVA-v1.6 (Liu et al., 2024b) and LLaVA-ov (Li et al., 2024a), segment images into multiple image crops. Each image crop is independently encoded using ViT (Dosovitskiy et al., 2021) and subsequently concatenated for LLM processing.

HR Visual Encoder. High-resolution image understanding can be enhanced by incorporating HR visual encoders without substantially increasing the number of visual tokens. For instance, Vary (Wei et al., 2023) and Deepseek-VL (Lu et al., 2024) adopt the SAM (Kirillov et al., 2023) to improve the performance of MLLMs on HR images. MiniGemini-HD (Li et al., 2024b), LLaVA-HR (Luo et al., 2024), and ConvLLaVA (Ge et al., 2024) utilize ConvNeXt (Liu et al., 2022), employing techniques such as cross-attention or adapter to extract visual features.

Search-Based Methods. Search-based methods organize images into a tree structure to extract query-relevant regions through a top-down approach. *DC*² (Wang et al., 2024c) leverages visual memory to store objects and coordinates, retrieving crops to generate text and reduce detail loss. Zoom Eye (Shen et al., 2024) employs a tree search algorithm to directly identify and extract relevant crops from HR images. Wu & Xie (2024) propose SEAL, a meta-architecture that actively reasons and retrieves essential visual information.

Multimodality RAG. Multimodal RAG tasks include matching images to text and retrieving text-image pairs to answer questions (Chang et al., 2022; Han et al., 2017; Xia et al., 2024a;b). Yu et al. (2024) propose Vision-based Retrieval-augmented Generation to effectively utilize and retain data in multimodal documents.

Existing methods enhance MLLMs’ ability to perceive HR images, but processing extremely HR images (e.g., 8K) remains challenging. Inspired by RAG’s success in handling long contexts for LLMs, this paper for the first time explores its use to improve MLLMs’ HR image perception.

3. Pilot Study

In this section, we conduct a systematic investigation into the challenges associated with employing RAG to enhance the perceptual capabilities of MLLMs, motivating the design of the proposed RAP framework in Sect. 4.

3.1. Preliminary

In this section, we introduce the pipeline for applying RAG to MLLMs for the perception of HR images. Given an HR image, we divide it into an image crop set, denoted as $V = \{v_1, \dots, v_n\}$, where n is the number of image crops. Inspired by Yu et al. (2024), the query and image crops are independently encoded as text and images within the VLM, yielding a sequence of hidden states. Subsequently, the similarity scores between the query embedding and the image crop embeddings are computed. The similarity score $s(q, V)$ is calculated by the cosine similarity of the query and image crop embeddings:

$$s(q, V) = (1 - \frac{q \cdot V^T}{\|q\| \cdot \|V\|}) \cdot \frac{1}{2}. \quad (1)$$

Finally, the top K image crops are selected based on the $s(q, V)$ to facilitate the MLLM’s perception of HR images.

In the following sections, we systematically analyze the impact of retrieved image crop layouts and quantities on *HR-Bench*, which consists of *HR-Bench 8K* and *HR-Bench 4K*. *HR-Bench 8K*, with 8K-resolution images from DIV8K (Gu et al., 2019) and the Internet, includes *Fine-grained Single-instance Perception (FSP)* and *Fine-grained Cross-instance Perception (FCP)* tasks. Cropping 8K images around relevant objects produces *HR-Bench 4K*.

3.2. Impact of the Layout of Retrieved Image Crops

This subsection investigates the relationship between the layout of retrieved image crops and the performance of MLLMs in the RAG system.

Experimental setting. We compare three layout strategies: 1) Sort according to the retrieval scores in ascending order; 2) After selecting the top K image crops, arrange them in the order in which the image crops appear; 3) Maintain the relative positional relationships of the image crops. We conduct experiments on *HR-Bench* using LLaVA-v1.6-7B.

Observations. As shown in Table 1, retrieving key image crops through RAG significantly improves performance on

Table 1. The effect of different layout strategies. While all three strategies improve fine-grained perception, only strategy 3) excels in *FCP* tasks by preserving positions, achieving superior performance compared to other strategies.

	HR-Bench 4K			HR-Bench 8K		
	<i>FSP</i>	<i>FCP</i>	Avg.	<i>FSP</i>	<i>FCP</i>	Avg.
Baseline	49.0	46.8	47.9	37.2	44.2	40.8
+ 1)	74.8	38.3	56.5	56.8	26.8	41.8
+ 2)	72.3	38.5	55.4	61.3	25.5	43.4
+ 3)	74.0	41.5	57.8	59.5	30.0	44.8

the *FSP* task but results in a noticeable performance drop on the *FCP* task. Furthermore, maintaining the relative positions between each image crop achieves a better performance balance between the *FSP* and *FCP* tasks.

Insights. Maintaining the relative positional relationships between retrieved image crops is essential, particularly for tasks requiring spatial awareness.

3.3. Impact of the Number of Retrieved Image Crops

This subsection investigates the relationship between the number of retrieved image crops and the performance of MLLMs in HR image perception.

Experimental setting. We analyze the relationship between performance (*i.e.*, accuracy) and the number of the retrieved image crops, using the LLaVA-v1.5 and LLaVA-v1.6.

Observations. As shown in Figure 2, we visualize the relationship between the number of retrieved image crops (*i.e.*, K) and performance. As K increases, more image crops are introduced, providing additional visual information that enhances performance on *FCP* tasks. However, this also raises the image resolution, increasing the likelihood of the model generating incorrect answers. Conversely, smaller K retains only essential visual information, improving performance on *FSP* tasks but sacrificing significant visual details, which causes a notable performance decline on *FCP* tasks.

Insights. Different types of tasks require different numbers of retrieved image crops K . For *FSP* tasks, smaller K improves results, but larger K reduces performance by increasing resolution. Conversely, for *FCP* tasks, larger K preserves visual information and outperforms smaller K .

4. Proposed Retrieval-Augmented Perception

4.1. Method Overview

Driven by the aforementioned insights in Sect. 3, we propose a novel framework — **Retrieval-Augmented Perception (RAP)**. The design principle of **RAP** is to retrieve key image

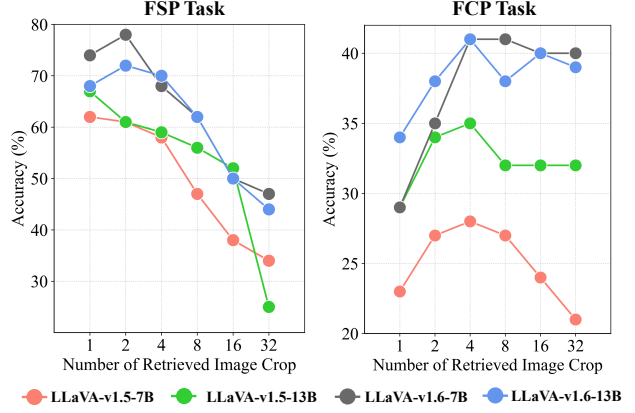


Figure 2. The effect of the number of retrieved image crops on model performance. *FSP* and *FCP* represent the fine-grained single-instance perception tasks and fine-grained cross-instance perception tasks, respectively.

crops to replace the original HR image, preserving essential visual information while reducing resolution to improve MLLM perception of HR images. To achieve this, we divide the image into various crops, calculate similarity scores (Eq. 1) with the query, and select the top K image crops to synthesize a new image V' . We design a *Spatial-Awareness Layout* algorithm to maintain the relative positional relationships between the image crops. To adaptively select K , we propose *Retrieved-Exploration Search (RE-Search)*, which determines K based on the model’s confidence in V' and its similarity to the query. The *Spatial-Awareness Layout* and *RE-Search* are presented in the subsequent sections.

4.2. Spatial-Awareness Layout

In Sect. 3.2, we find that maintaining the positional relationship between image crops is essential. Thus, we propose a simple and efficient method, termed *Spatial-Awareness Layout*. We denote $M \in \{0, 1\}^{R \times C}$ as a binary matrix of size $R \times C$, where R and C represent the number of rows and columns of image crops V , respectively. The $M_{i,j} = 1$ indicates an image crop to be preserved and $M_{i,j} = 0$ indicates the image crops to be removed. We seek to construct a compressed matrix M' by removing any row or column of M that is entirely zero. Formally, we define two index sets:

$$R' = \{i | \exists j \text{ s.t. } M_{i,j} = 1\}, C' = \{j | \exists i \text{ s.t. } M_{i,j} = 1\}. \quad (2)$$

The compressed matrix $M' \in \{0, 1\}^{N_r \times N_c}$, with $N_r = |R'|$ and $N_c = |C'|$, is then constructed according to: $M'_{\tilde{i}, \tilde{j}} = M_{i,j}$, where $i = R'[\tilde{i}]$ and $j = C'[\tilde{j}]$. This guarantees that M' retains all rows and columns of M containing at least one entry equal to 1, effectively discarding rows and columns composed entirely of zeros. Moreover, an mapping function $\Phi : \{0, \dots, N_r - 1\} \times \{0, \dots, N_c - 1\} \rightarrow \{0, \dots, R - 1\} \times \{0, \dots, C - 1\}$ is defined as $\Phi(\tilde{i}, \tilde{j}) = (R'[\tilde{i}], C'[\tilde{j}])$, thereby enabling each coordinate (\tilde{i}, \tilde{j}) in the compressed

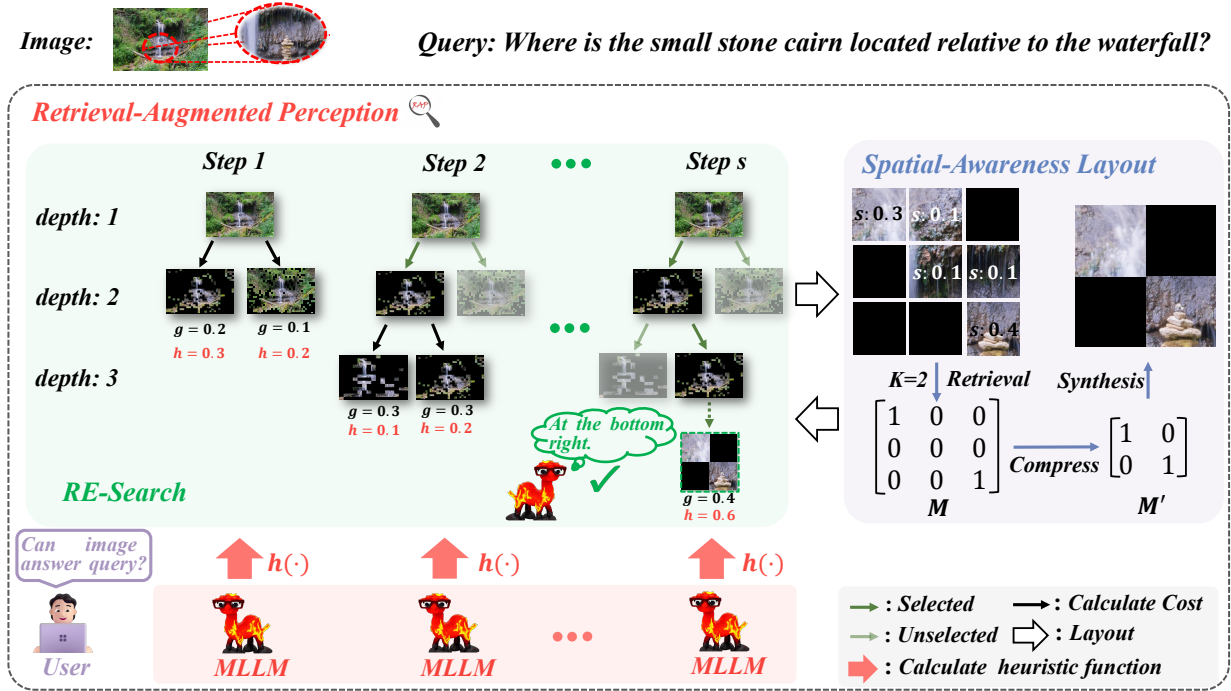


Figure 3. Detailed illustration of our proposed **RAP** with a running example. We firstly divide HR image into multiple image crops and compute the similarity score s between the query and image crops to retrieve the key image crops. We design a simple and efficient method called **Spatial-Awareness Layout** to maintain the relative positional relationships of the image crops. Since the number of image crops is highly sensitive to the task type, we propose **RE-Search**, which identifies the optimal K based on the model’s confidence scores and retrieval scores.

matrix M' to be mapped back to its original position (i, j) in M . Finally, we initialize an blank image V' and iterates over the mapping Φ , where each pair (\hat{i}, \hat{j}) is mapped to (i, j) . For each mapping, $V[\hat{i}][\hat{j}]$ is assigned to the corresponding $V'[i][j]$. We use image V' to replace the HR image V for the MLLM to answer the query. The implement of **Spatial-Awareness Layout** is shown in Algorithm 1.

4.3. Retrieved-Exploration Search

In Sect. 3.3, we find that different types of tasks significantly influence the choice of K . Here, we utilize a search algorithm to obtain the optimal K . For search algorithm, we consider two primary factors: **Efficiency**, ensuring high efficiency for optimal user experience, and **Robustness**, guaranteeing consistent results across multiple runs in image perception tasks. Existing tree-search methods (Wang et al., 2024c) require visiting all nodes, leading to low efficiency. With the development of O1, many recent works (Yao et al., 2024; Zhao et al.) employ Monte Carlo Tree Search (MCTS) to find the optimal reasoning path. However, MCTS relies on random sampling, resulting in a lower robustness. A^* search algorithm uses a heuristic function to intelligently guide its exploration. This heuristic allows A^* to prioritize promising paths, significantly accelerating the search

process. Furthermore, A^* explores the nodes in the same order and find the same optimal path, ensures high robustness. However, effectively defining the state representation and designing an appropriate heuristic function for A^* is a non-trivial challenge.

Building upon the strengths of A^* , we introduce **Retrieved-Exploration Search (RE-Search)**. In the following parts, we will elucidate the RE-Tree, a novel structure that elegantly represents the search states within **RE-Search**, and the REward function, which serves as the guiding heuristic for this innovative approach.

RE-Tree Representation. Inspired by Wang et al. (2024c); Shen et al. (2024), we model the HR image as a tree. Unlike existing search-based methods, we represent distinct nodes at the same layer by preserving different K image crops. This enables the model to perceive lower-resolution images from the beginning, mitigating the risk of the MLLM converging to suboptimal solutions. We denote $P = \{p_1, \dots, p_n\}$ as the retention ratio. For instance, for the first child node n_1 , we retain the top $N' \times p_1$ image crops. The N' represents the number of image crops for the current image. To obtain a complete image for calculating the REward function, we employ **Spatial-Awareness Layout** to assemble the individual image crops into a complete image V' .

Algorithm 1 Spatial-Awareness Layout

```

function SpatialLayout( $V, M$ )
     $R' \leftarrow \{i \mid \exists j \text{ s.t. } M_{i,j} = 1\}$ 
     $C' = \{j \mid \exists i \text{ s.t. } M_{i,j} = 1\}$ 
     $N_r \leftarrow |R'|, \quad N_c \leftarrow |C'|$ 
    Construct a binary matrix  $M' \in \{0, 1\}^{N_r \times N_c}$ 
    for  $\tilde{i} = 1 \rightarrow N_r - 1$  do
        for  $\tilde{j} = 0 \rightarrow N_c - 1$  do
             $i \leftarrow R'[\tilde{i}], \quad j \leftarrow C'[\tilde{j}]$ 
             $M'_{\tilde{i}, \tilde{j}} \leftarrow M_{i,j}$ 
        end for
    end for
    Initialize a blank image  $V'$ 
    for  $\tilde{i} = 0 \rightarrow N_r - 1$  do
        for  $\tilde{j} = 0 \rightarrow N_c - 1$  do
             $i \leftarrow R'[\tilde{i}], \quad j \leftarrow C'[\tilde{j}]$ 
            if  $M'_{\tilde{i}, \tilde{j}} = 1$  then
                 $V'[\tilde{i}, \tilde{j}] \leftarrow V[i, j]$ 
            end if
        end for
    end for
    return  $V'$ 
end function
    
```

REward Function. A^* search is a best-first search algorithm that prioritizes nodes with the lowest combined cost, calculated as the sum of the actual cost $g(t_s)$ from the start node t_0 to t_s and the estimated cost $h(t_s)$ to the goal. In our *RE-Search*, the path from t_0 to t_s is represented as the progression from the original HR image to the currently retained top- K image crops. We use the similarity score between these K image crops and the query as $g(t_s)$:

$$g(t_s) = \frac{1}{n} \sum_{i=1}^n s(q, v_i), \quad (3)$$

where n represents the number of image crops, and v_i represents the i -th image crops for current image V . Inspired by Shen et al. (2024), we use the model’s confidence in whether the current image V can answer the given query as the cost from t_s to the goal:

$$h(t_s) = 1 - \mathcal{P}_\theta(\text{“Yes”} | p_h(q), V), \quad (4)$$

where \mathcal{P}_θ represents the MLLM and $p_h(\cdot)$ represents the prompt (e.g., “Question: $\{q\}$. Could you answer the question based on the available visual information? Answer Yes or No.”) used to query the MLLM for calculating the confidence that the answer is “Yes”. We utilize the model’s confidence to estimate the cost from the current to the target node, analogous to the heuristic function in the A^* algorithm. A lower $h(\cdot)$ indicates a higher likelihood of containing essential information, warranting prioritized exploration.

Since MLLM cannot accurately perceive the HR image at the beginning, the $h(t_s)$ provided at shallow depths of the tree is unreliable. As the tree depth increases and the image resolution gradually decreases, the model becomes more confident in determining whether the current image can answer the query. Therefore, we assign a lower weight to $h(t_s)$ at the beginning and gradually increase its weight as the tree depth grows. Mathematically, the cost function $f(t)$ can be written as:

$$f(t_s) = (1 - w) \cdot g(t_s) + w \cdot h(t_s), \quad (5)$$

$$w = (1 - b) \cdot (1 - \frac{1}{d})^2 + b, \quad (6)$$

where b is a bias value, set here at 0.2 and d denotes the depth of the image tree.

4.4. Algorithmic Workflow

In this section, we introduce how to use our **RAP** to perceive HR image. Given a HR image I , we first divide the HR image into various image crops V , with the size of each image crop not exceeding the predefined resolution of the retriever’s image encoder. Subsequently, we utilize VisRAG (Yu et al., 2024) to compute the cosine similarity between the query and image crops. We use *RE-Search* to search the optimal K image crops and using the *Spatial-Awareness Layout* to synthesize the image V_f , which replaces the original HR image V as input to the MLLM. We denote c as the answering confidence which is calculated by Eq. 4. When c exceeds a predefined threshold τ , the search terminates. We set $\tau = 0.6$ throughout the paper.

5. Experiments

5.1. Results on HR Benchmark

Benchmarks. We evaluate our **RAP** on two HR benchmarks: **V^* Bench** and **HR-Bench**. **V^* Bench**, derived from SA-1B (Kirillov et al., 2023), averages a resolution of 2246×1582 . More details about **HR-Bench** can be found in Sect. 3.1.

Main Results. As shown in Table 2, compared to the baseline MLLM, the performance of nearly all models significantly improved with our **RAP**, demonstrating the model-agnostic trait of **RAP**. We find that our **RAP** can bring significant improvements in both **FSP** and **FCP** tasks. Our **RAP** brings a maximum of 21.0% and 21.7% accuracy improvement on **HR-Bench 4K** and **HR-Bench 8K** respectively. Additionally, for tasks requiring spatial reasoning capabilities, **RAP** demonstrates significant improvements compared to the baseline (e.g., +39.5% accuracy on **V^* Bench** using LLaVA-v1.5-7B). The results show that our method has a clear advantage with HR images.

Table 2. Comparison of our **RAP** (upon several advanced models) with existing works on high-resolution benchmarks. The best performance in each task is in-bold.

Method	<i>V* Bench</i>			<i>HR-Bench 4K</i>			<i>HR-Bench 8K</i>		
	<i>Attribute</i>	<i>Spatial</i>	<i>Overall</i>	<i>FSP</i>	<i>FCP</i>	<i>Overall</i>	<i>FSP</i>	<i>FCP</i>	<i>Overall</i>
<i>Open-source MLLMs</i>									
LLaVA-v1.6-7B (Liu et al., 2024b)	60.9	63.2	61.8	49.0	46.8	47.9	37.3	44.3	40.8
LLaVA-v1.6-13B (Liu et al., 2024b)	60.0	64.5	61.8	49.8	41.3	45.5	38.0	38.3	38.1
LLaVA-v1.6-34B (Liu et al., 2024b)	-	-	-	55.3	50.5	52.9	44.5	50.3	47.4
LLaVA-HR-X-13B (Luo et al., 2024)	-	-	-	61.3	46.0	53.6	49.5	44.3	46.9
LLaVA-HR-X-7B (Luo et al., 2024)	51.3	64.5	56.5	57.8	46.3	52.0	42.0	41.3	41.6
InternVL-1.5-26B (Chen et al., 2024b)	-	-	-	69.5	51.8	60.6	69.3	48.5	57.9
Yi-VL-34B (Young et al., 2024)	-	-	-	46.0	42.8	44.4	39.5	38.5	39.0
<i>Closed-source MLLMs</i>									
GPT 4o (Hurst et al., 2024)	-	-	66.0	70.0	48.0	59.0	62.0	49.0	55.5
QWen-VL-max (Bai et al., 2023)	-	-	-	65.0	52.0	58.5	54.0	51.0	52.5
<i>Baseline and RAP</i>									
LLaVA-v1.5-7B (Liu et al., 2024a)	43.5	56.6	48.7	38.5	33.8	36.1	33.0	31.3	32.1
-w/ RAP	90.4	96.1	91.1	73.8	40.5	57.1	72.3	35.3	53.8
LLaVA-v1.5-13B (Liu et al., 2024a)	41.7	55.3	47.1	45.2	41.3	43.3	37.5	38.0	37.8
-w/ RAP	89.6	90.8	89.8	74.3	46.0	60.1	76.5	42.0	59.3
LLaVA-ov-0.5B (Li et al., 2024a)	63.5	64.5	63.9	63.5	39.5	51.5	47.3	38.3	42.8
-w/ RAP	80.0	84.2	83.6	80.3	42.3	61.3	81.8	45.3	63.5

5.2. Results on General Multimodal Benchmark

Benchmark. We conduct additional evaluations of **RAP** using the MME-RealWorld (Zhang et al., 2024c), a manually curated benchmark designed for partial, real-world scenarios. This benchmark encompasses five primary categories and 43 sub-class tasks. Due to space constraints, we present results for 9 sub-tasks that exhibit notable performance variations with **RAP**.

Main Results. As shown in Table 3, **RAP** improves the performance of LLaVA-v1.5-13B on most sub-tasks, especially on MO/Orientation (+7.3%), AD/Intention (+6.0%), and OCR/license (+10.3%). However, we observe that tasks involving Diagram and Table types do not exhibit significant improvements and, in some cases, even performance degradation. We find that this due to the reliance of such data on the model’s spatial awareness and reasoning capabilities, which are inherent limitations of current MLLMs.

5.3. Ablation Study

To better understand the role of each module in our **RAP**, we conduct ablation study on **HR-Bench 8K** using LLaVA-v1.5-7B. As shown in Table 4, we first use VisRAG to retrieve key image crops, replacing the original HR images, resulting in an average improvement of 4.5% accuracy compared to the baseline. However, we find a significant improvement in the **FSP** task, but there is a noticeable performance drop in the **FCP** task. By incorporating the *Spatial-Awareness*

Layout, the relative positional relationships between image crops are preserved, leading to an improvement in accuracy on the **FCP** task compared to **+VisRAG**. Finally, we utilize *RE-Search* to determine the optimal K for different samples, resulting in significant improvements in both the **FSP** and **FCP** tasks, with an average improvement of 21.7% accuracy compared to the baseline.

5.4. Performance and Efficiency

Efficiency concerns regarding **RAP** may arise among researchers. To address this, Table 5 presents a comparative analysis of throughput and accuracy against SOTA search-based methods (e.g., DC² and Zoom Eye). **RAP** achieves superior efficiency and performance by directly computing the relevance between image crops and the query, eliminating the need for hierarchical image partitioning, thereby significantly accelerating the search process.

5.5. Why Does Our Method Work?

Reviewing the design principles of **RAP**: Retrieve image crops related to the query to reduce the image resolution input to the MLLM, thereby enabling the MLLM to perceive images more accurately. To explore the underlying mechanism of **RAP**, we perform experiments that help address the following questions:

1) Is it truly necessary to retrieve image crops relevant to the query? we compare randomly retained image crops

Table 3. Comparison of the **RAP** against the baseline MLLM on the MME-RealWorld benchmark. MO: Monitoring; AD: Autonomous Driving. The “ $\Delta(\uparrow)$ ” represents the performance gains of our RAP against the baselines.

Method	MO			AD			OCR		
	Property	Orientation	Color	Intention	Attention	Visual	license	Text	Address
LLaVA-v1.5-13B	31.0	14.7	21.9	16.6	27.2	36.3	46.6	46.0	39.7
-w/ RAP	38.0	22.1	27.8	22.6	31.3	42.3	56.9	52.5	45.1
$\Delta(\uparrow)$	+7.0	+7.3	+5.9	+6.0	+4.2	+6.0	+10.3	+6.5	+5.4

Table 4. Ablation study of different module in **RAP**. “**SL**” denotes our *Spatial-Awareness Layout*. We first incorporate VisRAG to retrieve K key image crops, where $K = 8$. Then, we add *Spatial-Awareness Layout* to preserve the relative positional information of the image crops. Finally, we incorporate *RE-Search* to search the optimal K .

	HR-Bench 8K			$\Delta(\uparrow)$
	FSP	FCP	Overall	
LLaVA-v1.5-7B	33.0	31.3	32.1	-
+ VisRAG	52.3	25.0	38.6	+6.5
+ SL	50.0	27.5	38.8	+6.8
+ RE-Search	72.3	35.3	53.8	+21.7

Table 5. Evaluation of performance and inference efficiency. We analyze the correlation between throughput (samples per minute) and accuracy of LLaVA-v1.5-13B enhanced with our **RAP**, comparing it against search-based methods on **HR-Bench 4K**.

Method	Throughput \uparrow	Accuracy \uparrow
DC ² (Wang et al., 2024c)	2.1	51.5
Zoom Eye (Shen et al., 2024)	3.3	58.0
RAP	4.2	60.1

with query-relevant image crops using LLaVA-v1.5-7B on **HR-Bench 8K**. As shown in Table 6, we randomly retained $K = 4$ and half of the image crops, comparing them with K image crops retrieved through VisRAG that are relevant to the query. The results indicate that **retaining query-relevant image crops is necessary**.

2) Can RAP accurately select an appropriate K ? To answer this question, we visualize the distribution of the number of retrieved image crops (K) for LLaVA-v1.5-7B w/ **RAP** on **HR-Bench 8K**. As shown in Figure 4(a), our **RAP** effectively reduces the number of image crops, resulting in a +21.7% accuracy improvement. Additionally, for the **FSP** task, the K selected by our **RAP** is smaller, while for the **FCP** task, it is widely distributed across the range corresponding to larger K (e.g., $K \geq 60$). The experiment results demonstrate that **our RAP can provide accurate K , thereby effectively reducing the image resolution**.

Table 6. Effect of retrieval on **HR-Bench 8K**. We compare two methods: randomly retaining K image crops (**Random**) and retrieving K image crops. The “half” refers to retaining half of the image crops (**Retrieval**).

Method	HR-Bench 8K		
	FSP	FCP	Avg.
Random ($K = 4$)	25.0	23.8	24.4
Random ($K = \text{half}$)	29.0	24.5	26.8
Retrieval ($K = 4$)	52.3	25.0	38.6

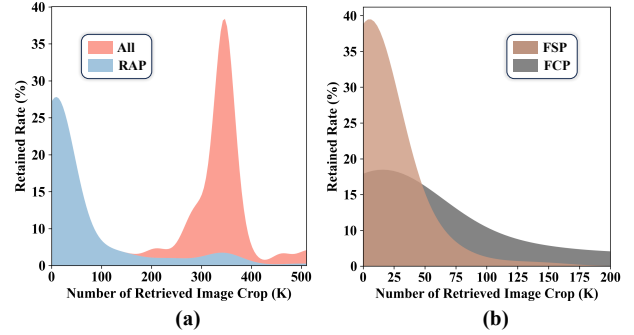


Figure 4. Analyzing the distribution for selecting K using our **RAP**. (a) The distribution of K selected by **RAP**, where “All” denotes the total number of image crops in the original image. (b) The distribution of K corresponding to different task types.

6. Conclusion

In this paper, we propose a novel training-free framework **Retrieval-Augmented Perception (RAP)** to enhance HR image understanding in MLLMs. We empirically demonstrated the effectiveness and universality of **RAP** on several widely used MLLM benchmarks. From the results, we mainly conclude that: (1) Retrieving image crops relevant to the query can result in significant improvements; (2) Maintaining the relative spatial relationships of the retrieved image crops is essential, particularly for tasks that rely on positional information; (3) The number of image crops that need to be retained varies across different task types. In our future work, we will explore more token compression techniques to further enhance HR perception and efficiency.

References

- Abdin, M., Jacobs, S. A., Awan, A. A., Aneja, J., Awadallah, A., Awadalla, H., Bach, N., Bahree, A., Bakhtiari, A., Behl, H., et al. Phi-3 technical report: A highly capable language model locally on your phone. *arXiv preprint*, 2024. URL <https://arxiv.org/abs/2404.14219>.
- Bai, J., Bai, S., Yang, S., Wang, S., Tan, S., Wang, P., Lin, J., Zhou, C., and Zhou, J. Qwen-vl: A versatile vision-language model for understanding, localization, text reading, and beyond. *arXiv preprint*, 2023. URL <https://arxiv.org/abs/2308.12966>.
- Chang, Y., Narang, M., Suzuki, H., Cao, G., Gao, J., and Bisk, Y. Webqa: Multihop and multimodal qa. In *Proceedings of the IEEE/CVF conference on computer vision and pattern recognition*, pp. 16495–16504, 2022.
- Chen, K., Thapa, R., Chalamala, R., Athiwaratkun, B., Song, S. L., and Zou, J. Dragonfly: Multi-resolution zoom supercharges large visual-language model. *arXiv preprint*, 2024a. URL <https://arxiv.org/abs/2406.00977>.
- Chen, Z., Wang, W., Tian, H., Ye, S., Gao, Z., Cui, E., Tong, W., Hu, K., Luo, J., Ma, Z., et al. How far are we to gpt-4v? closing the gap to commercial multimodal models with open-source suites. *arXiv preprint*, 2024b. URL <https://arxiv.org/abs/2404.16821>.
- Dosovitskiy, A., Beyer, L., Kolesnikov, A., Weissenborn, D., Zhai, X., Unterthiner, T., Dehghani, M., Minderer, M., Heigold, G., Gelly, S., Uszkoreit, J., and Houshy, N. An image is worth 16x16 words: Transformers for image recognition at scale. In *ICLR*, 2021. URL <https://openreview.net/forum?id=YicbFdNTTy>.
- Ge, C., Cheng, S., Wang, Z., Yuan, J., Gao, Y., Song, J., Song, S., Huang, G., and Zheng, B. Convllava: Hierarchical backbones as visual encoder for large multimodal models. *arXiv preprint*, 2024. URL <https://arxiv.org/abs/2405.15738>.
- Gu, S., Lugmayr, A., Danelljan, M., Fritsche, M., Lamm, J., and Timofte, R. Div8k: Diverse 8k resolution image dataset. In *ICCVW*, 2019. URL <https://ieeexplore.ieee.org/abstract/document/9021973>.
- Han, X., Wu, Z., Huang, P. X., Zhang, X., Zhu, M., Li, Y., Zhao, Y., and Davis, L. S. Automatic spatially-aware fashion concept discovery. In *ICCV*, pp. 1463–1471, 2017. URL https://openaccess.thecvf.com/content_iccv_2017/html/Han_Automatic_Spatially-Aware_Fashion_ICCV_2017_paper.html.
- Hurst, A., Lerer, A., Goucher, A. P., Perelman, A., Ramesh, A., Clark, A., Ostrow, A., Welihinda, A., Hayes, A., Radford, A., et al. Gpt-4o system card. *arXiv preprint*, 2024. URL <https://arxiv.org/abs/2410.21276>.
- Jin, B., Yoon, J., Han, J., and Arik, S. O. Long-context llms meet rag: Overcoming challenges for long inputs in rag. *arXiv preprint*, 2024. URL <https://arxiv.org/abs/2410.05983>.
- Jing, Y., Yang, Y., Wang, X., Song, M., and Tao, D. Meta-aggregator: Learning to aggregate for 1-bit graph neural networks. In *Proceedings of the IEEE/CVF international conference on computer vision*, pp. 5301–5310, 2021a. URL https://openaccess.thecvf.com/content/ICCV2021/html/Jing_Meta-Aggregator_Learning_To_Aggregate_for_1-Bit_Graph_Neural_Networks_ICCV_2021_paper.html.
- Jing, Y., Yang, Y., Wang, X., Song, M., and Tao, D. Turning frequency to resolution: Video super-resolution via event cameras. In *Proceedings of the IEEE/CVF Conference on Computer Vision and Pattern Recognition*, pp. 7772–7781, 2021b. URL https://openaccess.thecvf.com/content/CVPR2021/html/Jing_Turning_Frequency_to_Resolution_Video_Super-Resolution_via_Event_Cameras_CVPR_2021_paper.html.
- Jing, Y., Yuan, C., Ju, L., Yang, Y., Wang, X., and Tao, D. Deep graph reprogramming. In *Proceedings of the IEEE/CVF Conference on Computer Vision and Pattern Recognition*, pp. 24345–24354, 2023. URL https://openaccess.thecvf.com/content/CVPR2023/html/Jing_Deep_Graph_Reprogramming_CVPR_2023_paper.html.
- Kirillov, A., Mintun, E., Ravi, N., Mao, H., Rolland, C., Gustafson, L., Xiao, T., Whitehead, S., Berg, A. C., Lo, W.-Y., et al. Segment anything. In *ICCV*, 2023. URL https://openaccess.thecvf.com/content/ICCV2023/html/Kirillov_SegmentAnything_ICCV_2023_paper.html.
- Li, B., Zhang, Y., Guo, D., Zhang, R., Li, F., Zhang, H., Zhang, K., Zhang, P., Li, Y., Liu, Z., et al. Llava-onevision: Easy visual task transfer. *arXiv preprint*, 2024a. URL <https://arxiv.org/abs/2408.03326>.
- Li, Y., Zhang, Y., Wang, C., Zhong, Z., Chen, Y., Chu, R., Liu, S., and Jia, J. Mini-gemini: Mining the potential of multi-modality vision language models. *arXiv preprint*, 2024b. URL <https://arxiv.org/abs/2403.18814>.

- Li, Z., Yang, B., Liu, Q., Ma, Z., Zhang, S., Yang, J., Sun, Y., Liu, Y., and Bai, X. Monkey: Image resolution and text label are important things for large multi-modal models. In *CVPR*, 2024c. URL https://openaccess.thecvf.com/content/CVPR2024/html/Li_Monkey_Image_Resolution_and_Text_Label_Are_Important_Things_for_CVPR_2024_paper.html.
- Liu, H., Li, C., Li, Y., and Lee, Y. J. Improved baselines with visual instruction tuning. In *CVPR*, 2024a. URL https://openaccess.thecvf.com/content/CVPR2024/html/Liu_Improved_Baselines_with_Visual_Instruction_Tuning_CVPR_2024_paper.html.
- Liu, H., Li, C., Li, Y., Li, B., Zhang, Y., Shen, S., and Lee, Y. J. Llava-next: Improved reasoning, ocr, and world knowledge, 2024b. URL <https://llava-vl.github.io/blog/2024-01-30-llava-next/>.
- Liu, H., You, Q., Han, X., Wang, Y., Zhai, B., Liu, Y., Tao, Y., Huang, H., He, R., and Yang, H. Infimhd: A leap forward in high-resolution multimodal understanding. *arXiv preprint*, 2024c. URL <https://arxiv.org/abs/2403.01487>.
- Liu, Z., Mao, H., Wu, C.-Y., Feichtenhofer, C., Darrell, T., and Xie, S. A convnet for the 2020s. In *CVPR*, 2022. URL https://openaccess.thecvf.com/content/CVPR2022/html/Liu_A_ConvNet_for_the_2020s_CVPR_2022_paper.html.
- Lu, H., Liu, W., Zhang, B., Wang, B., Dong, K., Liu, B., Sun, J., Ren, T., Li, Z., Yang, H., Sun, Y., Deng, C., Xu, H., Xie, Z., and Ruan, C. Deepseek-vl: Towards real-world vision-language understanding, 2024. URL <https://arxiv.org/abs/2403.05525>.
- Luo, G., Zhou, Y., Zhang, Y., Zheng, X., Sun, X., and Ji, R. Feast your eyes: Mixture-of-resolution adaptation for multimodal large language models. *arXiv preprint*, 2024. URL <https://arxiv.org/abs/2403.03003>.
- Radford, A., Kim, J. W., Hallacy, C., Ramesh, A., Goh, G., Agarwal, S., Sastry, G., Askell, A., Mishkin, P., Clark, J., et al. Learning transferable visual models from natural language supervision. In *ICML*, 2021. URL <https://proceedings.mlr.press/v139/radford21a>.
- Rao, J., Wang, F., Ding, L., Qi, S., Zhan, Y., Liu, W., and Tao, D. Where does the performance improvement come from? -a reproducibility concern about image-text retrieval. In *Proceedings of the 45th international ACM SIGIR conference on research and development in information retrieval*, pp. 2727–2737, 2022.
- Shen, H., Zhao, K., Zhao, T., Xu, R., Zhang, Z., Zhu, M., and Yin, J. Zoomeye: Enhancing multimodal llms with human-like zooming capabilities through tree-based image exploration. *arXiv preprint*, 2024. URL <https://arxiv.org/abs/2411.16044>.
- Touvron, H., Lavril, T., Izacard, G., Martinet, X., Lachaux, M.-A., Lacroix, T., Rozière, B., Goyal, N., Hambro, E., Azhar, F., et al. Llama: Open and efficient foundation language models. *arXiv preprint*, 2023a. URL <https://arxiv.org/abs/2302.13971>.
- Touvron, H., Martin, L., Stone, K., Albert, P., Almahairi, A., Babaei, Y., Bashlykov, N., Batra, S., Bhargava, P., Bhosale, S., et al. Llama 2: Open foundation and fine-tuned chat models. *arXiv preprint*, 2023b. URL <https://arxiv.org/abs/2307.09288>.
- Wang, F., Ding, L., Rao, J., Liu, Y., Shen, L., and Ding, C. Can linguistic knowledge improve multimodal alignment in vision-language pretraining? *ACM Transactions on Multimedia Computing, Communications and Applications*, 20(12):1–22, 2024a.
- Wang, R., Song, S., Ding, L., Gu, S. S., Gong, M., Iwasawa, Y., Matsuo, Y., and Guo, J. Mma: Benchmarking multimodal large language model in ambiguity contexts. 2025.
- Wang, W., Lv, Q., Yu, W., Hong, W., Qi, J., Wang, Y., Ji, J., Yang, Z., Zhao, L., Song, X., Xu, J., Xu, B., Li, J., Dong, Y., Ding, M., and Tang, J. Cogvlm: Visual expert for pretrained language models, 2023a. URL <https://arxiv.org/abs/2311.03079>.
- Wang, W., Ding, L., Shen, L., Luo, Y., Hu, H., and Tao, D. Wisdom: Improving multimodal sentiment analysis by fusing contextual world knowledge. In *Proceedings of the 32nd ACM International Conference on Multimedia*, MM ’24, pp. 2282–2291, New York, NY, USA, 2024b. Association for Computing Machinery. ISBN 9798400706868. doi: 10.1145/3664647.3681403. URL <https://doi.org/10.1145/3664647.3681403>.
- Wang, W., Ding, L., Zeng, M., Zhou, X., Shen, L., Luo, Y., and Tao, D. Divide, conquer and combine: A training-free framework for high-resolution image perception in multimodal large language models. *arXiv preprint*, 2024c. URL <https://arxiv.org/abs/2408.15556>.
- Wang, X., Li, X., Ding, L., Zhao, S., and Biemann, C. Using self-supervised dual constraint contrastive learning for cross-modal retrieval. In *ECAI*, pp. 2552–2559, 2023b.
- Wang, X., Pan, J., Ding, L., and Biemann, C. Mitigating hallucinations in large vision-language models with instruction contrastive decoding. In *Findings of the Association for Computational Linguistics ACL 2024*, pp. 15840–15853, 2024d.

- Wei, H., Kong, L., Chen, J., Zhao, L., Ge, Z., Yang, J., Sun, J., Han, C., and Zhang, X. Vary: Scaling up the vision vocabulary for large vision-language models. *arXiv preprint*, 2023. URL <https://arxiv.org/abs/2312.06109>.
- Wu, P. and Xie, S. V*: Guided visual search as a core mechanism in multimodal llms. In *CVPR*, 2024. URL https://openaccess.thecvf.com/content/CVPR2024/html/Wu_V_Guided_Visual_Search_as_a_Core_Mechanism_in_Multimodal_CVPR_2024_paper.html.
- Xia, P., Zhu, K., Li, H., Wang, T., Shi, W., Wang, S., Zhang, L., Zou, J., and Yao, H. Mmed-rag: Versatile multimodal rag system for medical vision language models. *arXiv preprint*, 2024a. URL <https://arxiv.org/abs/2410.13085>.
- Xia, P., Zhu, K., Li, H., Zhu, H., Li, Y., Li, G., Zhang, L., and Yao, H. Rule: Reliable multimodal rag for factuality in medical vision language models. In *EMNLP*, pp. 1081–1093, 2024b. URL <https://aclanthology.org/2024.emnlp-main.62/>.
- Yao, H., Huang, J., Wu, W., Zhang, J., Wang, Y., Liu, S., Wang, Y., Song, Y., Feng, H., Shen, L., et al. Mulberry: Empowering mllm with ol-like reasoning and reflection via collective monte carlo tree search. *arXiv preprint*, 2024. URL <https://arxiv.org/abs/2412.18319>.
- Yin, S., Fu, C., Zhao, S., Li, K., Sun, X., Xu, T., and Chen, E. A survey on multimodal large language models. *arXiv preprint*, 2023. URL <https://arxiv.org/abs/2306.13549>.
- Young, A., Chen, B., Li, C., Huang, C., Zhang, G., Zhang, G., Li, H., Zhu, J., Chen, J., Chang, J., et al. Yi: Open foundation models by 01. ai. *arXiv preprint*, 2024. URL <https://arxiv.org/abs/2403.04652>.
- Yu, S., Tang, C., Xu, B., Cui, J., Ran, J., Yan, Y., Liu, Z., Wang, S., Han, X., Liu, Z., et al. Visrag: Vision-based retrieval-augmented generation on multi-modality documents. *arXiv preprint*, 2024. URL <https://arxiv.org/abs/2410.10594>.
- Zhai, X., Mustafa, B., Kolesnikov, A., and Beyer, L. Sig-moid loss for language image pre-training. In *Proceedings of the IEEE/CVF international conference on computer vision*, pp. 11975–11986, 2023.
- Zhang, H., Wang, W., and Yu, T. Towards robust multimodal sentiment analysis with incomplete data. In *The Thirty-eighth Annual Conference on Neural Information Processing Systems*. URL <https://openreview.net/forum?id=mYEjc7qGRA>.
- Zhang, Y., Liu, Y., Guo, Z., Zhang, Y., Yang, X., Chen, C., Song, J., Zheng, B., Yao, Y., Liu, Z., et al. Llava-uhd v2: an mllm integrating high-resolution feature pyramid via hierarchical window transformer. *arXiv preprint*, 2024a. URL <https://arxiv.org/abs/2412.13871>.
- Zhang, Y.-F., Wen, Q., Fu, C., Wang, X., Zhang, Z., Wang, L., and Jin, R. Beyond llava-hd: Diving into high-resolution large multimodal models. *arXiv preprint*, 2024b. URL <https://arxiv.org/abs/2406.08487>.
- Zhang, Y.-F., Zhang, H., Tian, H., Fu, C., Zhang, S., Wu, J., Li, F., Wang, K., Wen, Q., Zhang, Z., et al. Mme-realworld: Could your multimodal llm challenge high-resolution real-world scenarios that are difficult for humans? *arXiv preprint*, 2024c. URL <https://arxiv.org/abs/2408.13257>.
- Zhao, Y., Yin, H., Zeng, B., Wang, H., Shi, T., Lyu, C., Wang, L., Luo, W., and Zhang, K. Marco-ol: Towards open reasoning models for open-ended solutions, 2024a. *arXiv preprint*. URL <https://arxiv.org/abs/2411.14405>.

Appendix

This appendix presents a detailed description of the proposed *Retrieval-Augmented Perception (RAP)*, along with additional results from **comprehensive experiments**, **ablation studies**, and **case analyses**. The structure of the appendix is summarized as follows.

- Appendix A provides the implementation details of *RAP*, including preprocessing and hyperparameter settings. Specifically, we introduce the specific implementation of the *Spatial-Awareness Layout* in Appendix A.1. Appendix A.2 presents the details of *RE-Search*, including the number of search steps and termination conditions. Finally, Appendix A.3 outlines the algorithmic workflow of the proposed *RAP*.
- Appendix B provides additional experimental results, including the impact of inference scaling (Appendix B.1), the influence of hyperparameters (Appendix B.2), the effect of the retriever (Appendix B.3), and a comprehensive comparison with search-based methods (Appendix B.4).
- Appendix C provides a qualitative analysis of the proposed *RAP* and the current SOTA methods (Wang et al., 2024c; Shen et al., 2024). Appendix C.1 presents qualitative analysis examples on the *fine-grained single-instance perception task*, while Appendix C.2 illustrates examples on the *fine-grained cross-instance perception task*.

A. Additional Implement Details

Due to space constraints in the main paper, additional implementation details are provided in this section. In Appendix A.1 and Appendix A.2, we elaborate on the implementation of *Spatial-Awareness Layout* and *Retrieved-Exploration Search*, respectively. Building upon these components, Appendix A.3 presents the complete algorithmic workflow of *Retrieval-Augmented Perception (RAP)*.

A.1. Implement Details of Spatial-Awareness Layout

Given an input image I , it is first partitioned into smaller image crops based on a predefined crop size, which corresponds to the preferred resolution of the retriever. To ensure that the image size are divisible by the crop size and to prevent potential loss of visual information, padding is applied to the original image I as necessary. Next, only non-zero image crops (referred to as *valid image crops*) are retained to eliminate potential interference in the subsequent semantic similarity computation with the query. The retriever, specifically VisRAG (Yu et al., 2024) in this implementation, is then utilized to compute the cosine similarity between the user-provided query and each valid image crop. Based on the given K , the top K image crops with the highest similarity scores are selected. Subsequently, the rows and columns containing the selected crops are retained, forming a compressed matrix M' . Finally, using M' , the corresponding image crops in I are mapped to construct a new transformed image I' .

A.2. Implement Details of Retrieved-Exploration Search

In *Retrieved-Exploration Search (RE-Search)*, a given HR image I is designated as the root node for the search process. The semantic similarity between I and the query is computed, along with an assessment of whether the image contains sufficient information for the MLLM to generate an appropriate response to the query. Subsequently, different proportions of image crops are retained based on the predefined retention ratio set P . Specifically, for each node, 25%, 50%, and 75% of the image crops are preserved. The REward function is then applied to the retained image crops, and corresponding child nodes are created. These child nodes are added to the list of candidate nodes \mathcal{O} for further exploration. Throughout the search process, the algorithm continuously tracks and maintains the optimal node identified thus far. The search process terminates if the current search step exceeds the predefined maximum search steps, which is set to 200 by default, or when the answering confidence c of the current node surpasses a specified threshold τ . We set $\tau = 0.6$ throughout the paper.

A.3. Complete of Algorithm Workflow

With the above notations and definitions in place, we provide the complete algorithm workflow in Algorithm 2.

Algorithm 2 *Retrieval-Augmented Perception*
Require: HR image I , Retriever R , Retention ratio P , Max steps max_s

 import *SpatialLayout* from Algorithm 1

function REward(q, I, d)

 $V : \{v_1, \dots, v_n\} \leftarrow$ Divide image I into image crops

 $g \leftarrow s(q, V)$
 $h \leftarrow 1 - \mathcal{P}_\theta(p_h(q), I)$
 $w \leftarrow (1 - b) \cdot (1 - \frac{1}{d})^2 + b$
 $f \leftarrow (1 - w) \cdot g + w \cdot h$

 return f
end function
function RetrievalSubNode(V)

 $V : \{v_1, \dots, v_n\} \leftarrow$ Divide image I into image crops

 Initialize $V_s \leftarrow \emptyset$

 Initialize $M_s \leftarrow \emptyset$
for $idx = 1$ to $|P|$ **do**
 $S \leftarrow s(q, V)$
 $V', M \leftarrow \text{topK}(S, V, P[idx])$
 $V_s \leftarrow V_s \cup \{V'\}$
 $M_s \leftarrow M_s \cup \{M\}$
end for

 return V_s, M_s
end function
 $f \leftarrow \text{REward}(q, I, 0)$
 $t_0 \leftarrow \text{Node}(v = I, f = f, d = 0)$

 Initialize $\mathcal{O} \leftarrow \{t_0\}$
 $t_{\text{optimal}} \leftarrow t_0$
 $S \leftarrow 0$ /*Current step */

while \mathcal{O} is not empty and $S \leq max_s$ **do**

 Extract all confidence $F \leftarrow [o.f : o \in \mathcal{O}]$
 $idx \leftarrow \arg \min(F)$
 $t_s \leftarrow \mathcal{O}[idx]$

 Remove t_s from \mathcal{O}
 $S \leftarrow S + 1$
if $t_s.f > \tau$ **then**

 return $t_{\text{optimal}}.v$
end if

/* Retrieval */

 $V_s, M_s \leftarrow \text{RetrievalSubNode}(I)$

/* Exploration */

for $idx = 1$ to $|V_s|$ **do**
 $I_s \leftarrow \text{SpatialLayout}(V_s[idx], M_s[idx])$
 $f_s \leftarrow \text{REward}(q, I_s, t_s.d)$
 $t_{s+1} \leftarrow \text{Node}(v = I_s, f = f_s, d = t_s.d + 1)$
 $\mathcal{O} \leftarrow \mathcal{O} \cup \{t_{s+1}\}$
if $t_{s+1}.f > t_{\text{optimal}}.f$ **then**
 $t_{\text{optimal}} \leftarrow t_{s+1}$
end if
end for
end while

B. More Experiment Result

B.1. RAP Performance and Inference Computation Scale

To analyze the performance changes with different search steps, we plot the performance of RE-Search steps. We conduct experiments on **HR-Bench 8K** using LLaVA-v1.5 7B & 13B, LLaVA-ov-0.5B. To accurately analyze the relationship between search steps and performance, we set $\tau = \infty$ to prevent early termination due to threshold constraints during the search process. This forces the model to perform a fixed number of steps and selects the K with the lowest cost as the final output. As shown in Figure 5, we observe that increasing the number of search steps improves the performance,

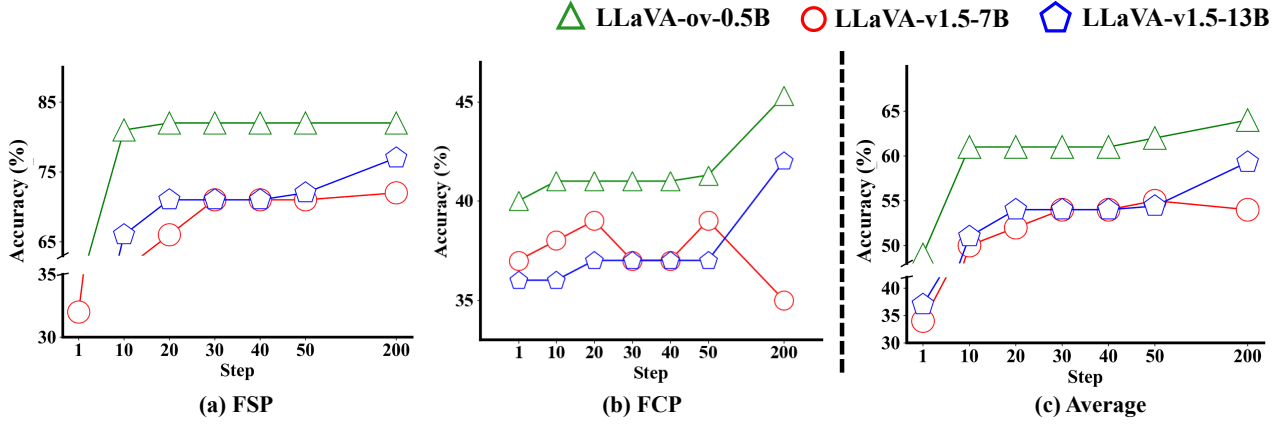


Figure 5. Performance vs. *RE-Search* steps on **HR-Bench 8K**. (a) *Fine-grained Single-instance Perception (FSP)*; (b) *Fine-grained Cross-instance Perception (FCP)*; (c) Overall Performance.

especially on the **FCP** task. However, the gains are marginal for LLaVA-v1.5-7B but more pronounced for stronger models like LLaVA-ov-0.5B and LLaVA-v1.5-13B. Our analysis reveals that the **FCP** task requires consideration of the spatial relationships between image crops and their spatial combinations, making capabilities result in a more noticeable performance improvement with increased search steps.

B.2. Effect of bias b

In the *RE-Search*, we use w to balance the cost $g(\cdot)$ and heuristic function $h(\cdot)$ in different depth. In Eq. 6, we use b as the bias value to control the influence of depth on w . A smaller b indicates a greater influence of depth on w , while a larger b reduces this influence.

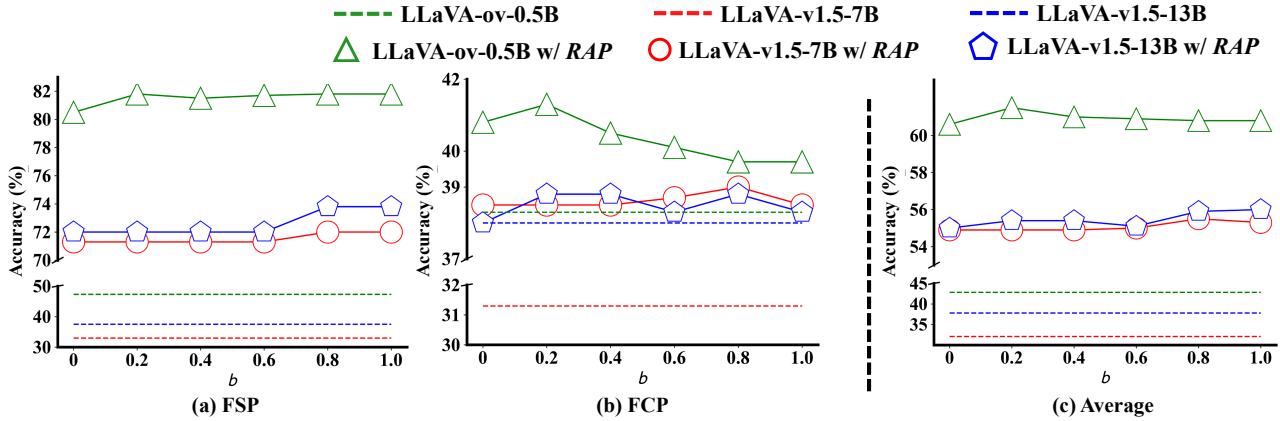


Figure 6. Impact of bias value b , illustrating how the accuracy changes when varying bias value b .

As shown in Figure 6, our **RAP** is not sensitive to the value of b , and it consistently outperforms the baseline across all configurations. Furthermore, we observe that smaller values of b lead to better results for all models. Therefore, to ensure a fair comparison, we set $b = 0.2$ by default.

B.3. Effect of Retriever

To explore the impact of retrieval quality on **RAP** performance, we conduct experiments on **HR-Bench 4K & 8K** using LLaVA-ov-0.5B with SigLIP (Zhai et al., 2023) and VisRAG (Yu et al., 2024). Due to the limited text input length of SigLIP, we utilize MLLM to extract noun phrases from the query to compute relevance with image crops.

As shown in Table 7, we evaluate the retrieval quality of SigLIP and VisRAG, finding that VisRAG achieves superior retrieval performance. Notably, our **RAP** significantly enhances performance even with the relatively weaker retriever (SigLIP); for instance, it delivers a 9.1% overall enhancement on **HR-Bench 8K**.

Table 7. Analyzing the relationship between **RAP** performance and retriever using LLaVA-ov-0.5B with SigLIP and VisRAG. The “Params.” refer to the total parameters of the retrievers. The evaluation results of DocVQA are measured using the retrieval metric MRR@10.

Method	Params.	DocVQA	HR-Bench 4K			HR-Bench 8K		
			FSP	FCP	Avg.	FSP	FCP	Avg.
LLaVA-ov-0.5B	-	-	63.5	39.5	51.5	47.3	38.3	42.8
w/ RAP (SigLIP)	883M	66.0	68.0	36.5	52.3	65.0	38.8	51.9
w/ RAP (VisRAG)	3.34B	77.7	80.3	42.3	61.3	81.8	45.3	63.5

B.4. Compared with Other HR Processing Methods

We compare our **RAP** with two HR processing methods – DC² and Zoom Eye. DC² is a training-free framework to enhance MLLM understanding of HR images by partitioning images, generating textual descriptions for image crops, and integrating them for improved perception. Zoom Eye, a tree search algorithm, is designed to effectively navigate the hierarchical and visual structures of images to extract relevant information.

As shown in Table 8, compared with the baseline, all HR processing methods bring the average performance gains. Among all these methods, our **RAP** achieves the relatively better formance on most tasks. For instance, **RAP** achieve an accuracy of 73.8% and 72.3% on **HR-Bench 4K** and **HR-Bench 8K**, respectively, using LLaVA-v1.5-7B, representing improvements of 6.0% and 6.8% compared to Zoom Eye. These results can prove the superiority of our **RAP**.

Table 8. Performance comparison between **RAP** and other HR methods. We conduct experiments on **V* Bench** and **HR-Bench** using LLaVA-v1.5 7B and 13B. The “ $\Delta(\uparrow)$ ” represents the performance gains of HR methods against the baselines.

Method	V* Bench			HR-Bench 4K			HR-Bench 8K			$\Delta(\uparrow)$
	Attribute	Spatial	Overall	FSP	FCP	Overall	FSP	FCP	Overall	
LLaVA-v1.5-7B	43.5	56.6	48.7	38.5	33.8	36.1	33.0	31.3	32.1	-
-w/ DC ²	49.6	59.2	51.6	45.3	37.0	41.1	36.5	33.3	34.9	+2.5
-w/ Zoom Eye	83.5	82.9	83.3	67.8	38.8	53.3	65.5	36.0	50.8	+22.5
-w/ RAP	90.4	96.1	91.1	73.8	40.5	57.1	72.3	35.3	53.8	+27.0
LLaVA-v1.5-13B	41.7	55.3	47.1	45.2	41.3	43.3	37.5	38.0	37.8	-
-w/ DC ²	54.8	56.6	57.3	52.0	51.0	51.5	40.0	41.0	40.5	+7.1
-w/ Zoom Eye	87.5	81.6	85.3	73.0	43.0	58.0	67.3	45.5	56.4	+23.9
-w/ RAP	89.6	90.8	89.8	74.3	46.0	60.1	76.5	42.0	59.3	+27.0

C. Case Study

C.1. Qualitative Examples of Fine-grained Single-instance Perception Task

Figure 7 illustrates two instances where incorporating different HR processing methods (DC^2 , Zoom Eye and our **RAP**) on LLaVA-v1.5-13B. In the first example, the critical information “08-26” in the image lies exactly at the boundary of two image crops. Zoom Eye retains only a part of it, leading to the loss of critical information. In contrast, our **RAP**, leveraging *RE-Search*, accurately preserves the critical information and provides a correct response. In the second example, DC^2 initially searches along an incorrect path, resulting in an erroneous final answer. In contrast, our **RAP** method accurately retrieves the cup on the ground, thereby providing the correct answer.

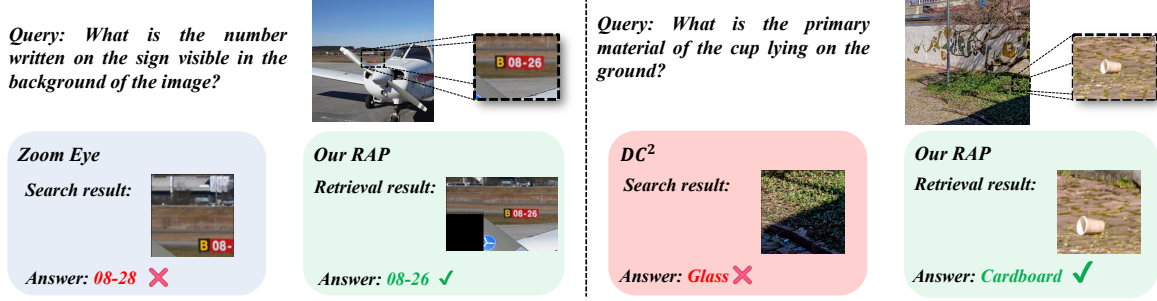


Figure 7. Qualitative examples of *Fine-grained Single-instance Perception* task. We conduct experiments on **HR-Bench 4K** using LLaVA-v1.5-13B with HR processing methods.

C.2. Qualitative Examples of Fine-grained Cross-instance Perception Task

Figure 8 presents two examples demonstrating the performance of different HR processing methods (DC^2 , Zoom Eye, and our **RAP**) applied to LLaVA-v1.5-13B. In the first example, Zoom Eye fails to consider the spatial relationships between image crops, leading to an incorrect search result and an erroneous response. In contrast, our **RAP** effectively preserves the relative positions between image crops, enabling the generation of a correct answer. In the second example, multiple image crops are required for accurate reasoning. However, DC^2 retrieves only a single image crop based on the keyword “chair” from the query, resulting in an incorrect answer. In contrast, our **RAP** accurately retains the critical image crops, thereby producing the correct answer.

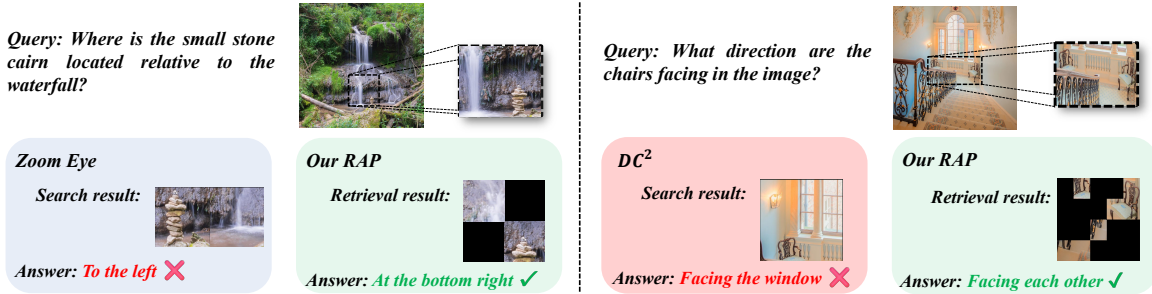


Figure 8. Qualitative examples of *Fine-grained Cross-instance Perception* task. We conduct experiments on **HR-Bench 4K** using LLaVA-v1.5 13B with HR processing methods.